

# Characterization of carbon nanotube–thermotropic nematic liquid crystal composites

O Trushkevych<sup>1</sup>, N Collings<sup>1</sup>, T Hasan<sup>1</sup>, V Scardaci<sup>1</sup>, A C Ferrari<sup>1</sup>,  
T D Wilkinson<sup>1</sup>, W A Crossland<sup>1</sup>, W I Milne<sup>1</sup>, J Geng<sup>2</sup>, B F G Johnson<sup>2</sup>  
and S Macaulay<sup>3</sup>

<sup>1</sup> Cambridge University, Engineering Department, 9 J J Thomson Avenue, Cambridge, CB3 0FA, UK

<sup>2</sup> Cambridge University, Chemistry Department, Lensfield Road, Cambridge CB2 1EW, UK

<sup>3</sup> Malvern Instruments Ltd, Enigma Business Park, Grovewood Road, Malvern, Worcestershire, WR14 1XZ, UK

E-mail: [ot213@cam.ac.uk](mailto:ot213@cam.ac.uk)

Received 23 October 2007, in final form 28 March 2008

Published 29 May 2008

Online at [stacks.iop.org/JPhysD/41/125106](http://stacks.iop.org/JPhysD/41/125106)

## Abstract

Dispersions of carbon nanotubes (CNTs) in liquid crystals (LCs) have attracted attention due to their unique properties and possible applications in photonics and electronics. However, these are hard to stabilize, and the loading level in the equilibrium state in LC hosts is small. A practical way to monitor the quality and CNT incorporation in such equilibrium dispersions is required. Here, we compare different methods for characterising equilibrium CNT–LC composite materials.

(Some figures in this article are in colour only in the electronic version)

## 1. Introduction

Liquid crystals (LCs) are highly anisotropic and easily switchable materials [1]. They are used in numerous applications especially in displays [1]. Carbon nanotubes (CNTs) are highly anisotropic materials. Aligned arrays or dispersions of CNTs could bring the attractive properties of the individual nanotubes on the macroscopic scale. CNTs dispersed in thermotropic nematic LCs may form well-aligned systems [2, 3]. Moreover, even small concentrations of CNTs in LC have been shown to lead to large nonlinear optical effects [4–6]. Enhancement of electro-optical as well as electrical and dielectric properties of the LC material has also been reported [7–9].

Techniques for dispersing CNTs in aqueous media and organic solvents are well developed [10–19]. These dispersions are usually stabilized against agglomeration by ions and surfactants [12, 14] or by covalent side-wall functionalization [20–22]. Concentrations may be as high as 1% weight [14–17].

Here, we study equilibrium CNT loaded thermotropic LCs. We find that when equilibrium is reached in the

dispersions, CNT concentration is very low. Different methods are used to characterize these CNT–LC dispersions.

## 2. Materials

We use as a LC host the commercially available thermotropic nematic material E7 from Merck [23]. In the rest of the paper we refer to thermotropic nematic LCs simply as LCs. We use the commercially available single-wall CNTs with octadecylamine (ODA) covalent side-wall functionalization from Sigma-Aldrich [24]. Octadecylamine is a long alkyl chain  $-\text{NHCH}_2(\text{CH}_2)_{16}\text{CH}_3$  and is appropriate for organic solvents. Because ODA is similar to the chains forming the nematic materials, one could expect this to promote CNT solubility in LC hosts.

Nanotubes are dispersed in LC using ultrasonication at 20 kHz for 5 h at 10–12 °C in an ultrasonicator from Diagenode (Bio-Ruptor). The power delivered to the bath is 300 W. CNTs settle out as dark residue, usually within 1–2 weeks after dispersing. Thus, the mixtures are left undisturbed for at least 2 weeks. The supernatant is then collected and filtered using

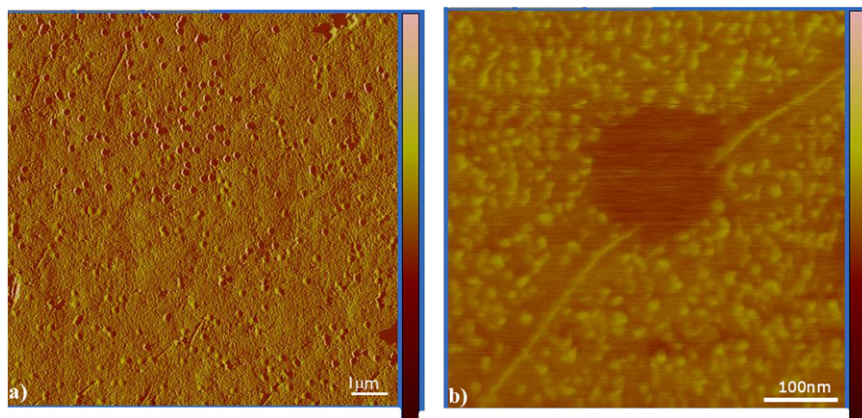


**Figure 1.** AFM images of (a) CNTs on filter (round spots are filter pores, fine and larger grooves—nanotubes and their bundles); (b) small CNT bundle seen across a filter pore (diameter  $\sim 6$  nm). Flow alignment and pressure during filtering pulls CNTs into (and possibly through) pores. Lighter spots—filter surface structure.

Whatman filters with  $5 \mu\text{m}$  pore size. The resulting dispersion is considered in equilibrium, as it does not form sediment in the course of months.

Due to the nature of the dispersing and filtering methods, the task of defining the exact concentration of CNTs in solution is far from straightforward. Weighting of substances before and after mixing does not give reliable information: the LC samples rarely weigh more than 1 g; the limitation of most scales is 0.01 mg (giving a minimum measurable percentage by weight (wt%) of 0.001%). Commercially available CNTs have purity usually of  $\sim 70$ – $90\%$  with main impurities in the form of catalyst metal, amorphous carbon and fullerenes. Also, there is a large amount of residue consisting mainly of CNT agglomerates. Our aim is to define a method to monitor nanotube loading in LC and the quality of the resulting dispersions.

### 3. Characterization methods for dilute equilibrium suspensions of CNTs in LCs

#### 3.1. Scanning probe microscopy

Atomic force microscopy (AFM), scanning electron microscopy (SEM) or environmental scanning electron microscopy (ESEM) and transmission electron microscopy (TEM) can all be used to image nanotubes. AFM and SEM/ESEM allow us to study the surface of the sample, and are not suitable for investigating bulk LC–CNT dispersions. For AFM characterization of LC–CNT dispersions, the use of planar membrane filters with small pore size, through which the LC–CNT mixture can be filtered, has been suggested in [3]. In this case CNTs remain as a residue. For AFM and ESEM characterization we use PTFE filters with pore size of  $0.2 \mu\text{m}$ . The LC–CNT mixture is encouraged to pass through the filter by vacuum suction, leaving CNTs on the filter. No solvent is used. Some LC host materials remain on the membranes.

AFM and SEM are most informative methods when a CNT dispersion is to be tested for particle size, concentration, agglomeration, bundling and alignment in an external electric field. Nevertheless, these have a number of limitations

including the small area that can be scanned in a given time ( $50 \times 50 \text{ nm}^2$  to resolve individual nanotubes), the difficulty of finding nanotubes if the solution is very dilute, the need to prepare special samples.

Note that CNT alignment with the LC host [2], which in turn is aligned by flow through the filter pores, may allow CNTs longer than the filter pore size to pass through. Also, CNTs shorter than the filter pore size would not be registered. Thus a systematic error is present in the measurement.

The AFM investigation (figure 1) is performed on the sample prepared using an equilibrated suspension of ODA functionalized SWNTs in LC. A MultiMode V with NanoScope V controller scanning probe microscope system from Veeco is used. In figure 1, the dots that look protruding are indentations—filter pores. We attribute the grooves (fine and larger ones) to nanotubes, either individual or in small bundles. The scale that allows statistical measurement of the CNTs length is too large for measuring the diameter of bundles and individual CNTs. Thus, as an example, we select one CNT bundle with average dimensions and take a high resolution scan of it (figure 1(b)). The measured diameter is 5 nm. Note that the CNT bundles are most certainly covered with LC and may be smaller than observed.

We distinguish  $\sim 70$  individual CNTs or small CNT bundles on a  $100 \mu\text{m}^2$  area of the filter. The effective area of the whole filter is  $1.15 \times 10^6 \mu\text{m}^2$ , and  $2 \mu\text{l}$  of suspension is filtered through it. Assuming that the distribution of nanotubes is uniform over the filter area, we may estimate a concentration  $\eta \sim 4 \times 10^8$  particles  $\text{ml}^{-1}$ . This corresponds to having approximately one nanotube or nanotube bundle per  $13.5 \times 13.5 \times 13.5 \mu\text{m}^3$  volume. The volume fraction of CNTs in LC host is  $\sim 4 \times 10^{-9}$  in the case of small bundles. The CNT bundles on average have 5 nm diameter ( $\sim 7$  nanotubes, 1.4 nm diameter each) and length  $0.5 \mu\text{m}$ . The corresponding molecular weight is  $M = 1.6 \times 10^6$ , and therefore there is  $\sim 7.4 \times 10^{-9}$  g of CNTs in 1 ml of dispersion. The density of E7 is  $\sim 1 \text{ g cm}^{-3}$  [25], therefore the weight fraction of CNTs bundles can be estimated as  $\sim 7.4 \times 10^{-9}$  wt. These figures are an approximation due to the uniform distribution assumption.

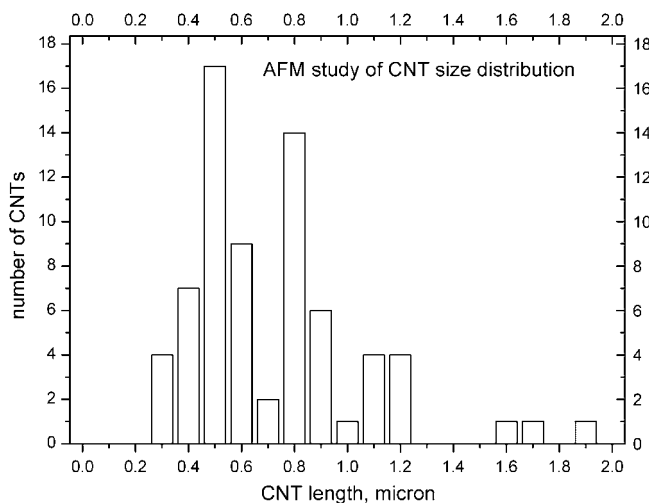


**Figure 2.** Distribution of CNTs by length (5 h of ultrasonication in LC host) from AFM studies.

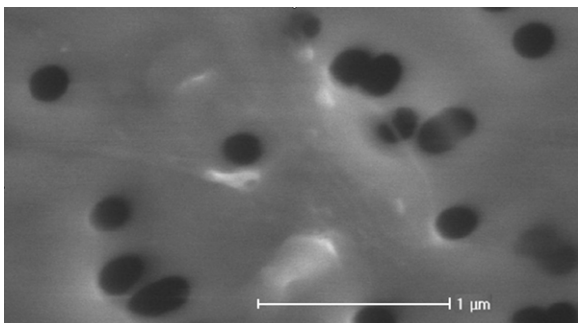


**Figure 3.** Single-wall CNTs/bundles imaged by ESEM technique at 5 kV and 1.4 Torr pressure. The round dots are filter pores while the lighter-coloured hair-like structures are CNTs and their bundles.

SEM studies are performed with a high resolution environmental scanning electron microscope (ESEM) FEI Philips XL30 FEG. The samples (same as for AFM) are charged under electron beam irradiation in vacuum. Thus an environmental SEM is needed. We use a 1.4 Torr vapour pressure to discharge the surface. CNTs can be seen on the filter through which the suspensions are passed (lighter hair-like structures in figure 3). We note that the images of CNTs produced with AFM are visually sharper and better suited for the analysis.

TEM is a powerful means for observing both the morphology and structure of CNTs. TEM studies are performed with a JEOL JEM-3011 electron microscope operated at 300 kV. A drop of the CNT loaded LCs is deposited on a 400 mesh Cu specimen grid coated with holey carbon. The grid is then placed in a sample holder and transferred into the microscope column. Images are recorded at magnifications up to  $\times 800\,000$ .

At the high resolutions needed to image our SWNTs, the scan area is typically less than  $1\ \mu\text{m} \times 1\ \mu\text{m}$ . In this technique, material is used as prepared (and we have already estimated that there is 1 bundle per  $\sim 13.5 \times 13.5 \times 13.5\ \mu\text{m}^3$  volume), hence the task of finding CNTs becomes very difficult, making TEM inefficient for concentration studies. We observe a large number of nanoparticles (indicated by arrows in figure 4(a)).

The diameter of the particles is typically  $\sim 1\text{--}3\ \text{nm}$ . High resolution TEM (HRTEM) reveals that they are single crystals with randomly oriented crystal lattice fringes (figure 4(b)). Almost certainly, these nanoparticles are the catalyst metals (metal impurities in the studied CNT material are estimated to be 4%wt by the manufacturer [24]). They seem to have significant solubility in LC.

Although not suitable for concentration studies, TEM is perhaps the best to monitor the quality and contamination of the CNT-LC composites on the smallest scale.

### 3.2. Optical microscopy

Large SWNT bundles and MWNTs may be directly imaged with a microscope [2]. More importantly, the LC director field may distort around particles or nanostructures, such as CNTs [22, 26], and this deformation of the nematic director field may be visible in polarized light, even though the particles may be smaller than the wavelength of visible light. By directly counting deformations of the director profile one can estimate the number of particles in the cell and therefore the impurity concentration. Therefore extremely low loading, as in our case, should be ideal for optical microscopic studies, producing a countable number of deformation centres.

We have studied homeotropically aligned (LC director perpendicular to the cell side) unloaded and CNT loaded LC  $20\ \mu\text{m}$  cells. Unloaded LC samples look uniformly black under crossed polarization. The cells filled with equilibrated LC-CNT mixtures exhibit visible deformations of the nematic director (bright dots and often crosses, figures 5(a) and (b)) that deform upon electric field application (up to 2 MHz frequency). The deformations are likely to be around the particles. It is impossible to judge whether those are individual nanotubes or bundles or large agglomerates of nanotubes or impurities.

The bright spots that we attribute to deformations from particles (assuming one particle per spot) are spaced about  $4\text{--}8\ \mu\text{m}$ . This corresponds to  $\sim 10^9$  particles  $\text{ml}^{-1}$ . If we assume that all of the observed deformations are due to CNTs or their bundles [26], using same numbers as in the similar calculation described in section 3.1 (CNTs of  $0.5\ \mu\text{m}$  length,  $1.4\ \text{nm}$  diameter,  $10^6$  molecular weight and LC of  $1\ \text{g ml}^{-1}$  density), this gives a volume fraction of  $8 \times 10^{-10}$  and weight fraction  $4 \times 10^{-9}$  wt (or  $\sim 10^{-8}$  wt if each particle is a small CNT bundle), which is consistent with our calculation of loading obtained from AFM studies for the same mixture.

From TEM we know that the studied CNT-LC dispersions contain metal catalyst particles (under  $1\text{--}3\ \text{nm}$  in diameter). The agglomerations of these particles (or other impurities) may contribute to the overall particle count and give an overestimated figure for the concentration.

### 3.3. Elastic light scattering

There are two main ways of determining particle size distribution in suspensions from the light they scatter. Both rely on measuring the Brownian motion of scattering particles, see, e.g. [28, 29]. The translational diffusion coefficient of a

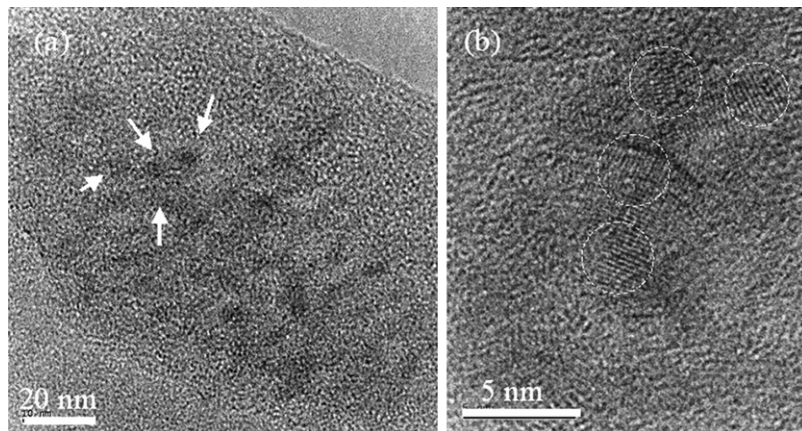


**Figure 4.** TEM observation of the metal impurities in the investigated mixture. (a): metal nanoparticles, marked by arrows; magnification  $\times 300\,000$ ; (b) randomly oriented crystal lattices of nanoparticles (1–3 nm, marked with circles), high resolution TEM image ( $\times 800\,000$ ).

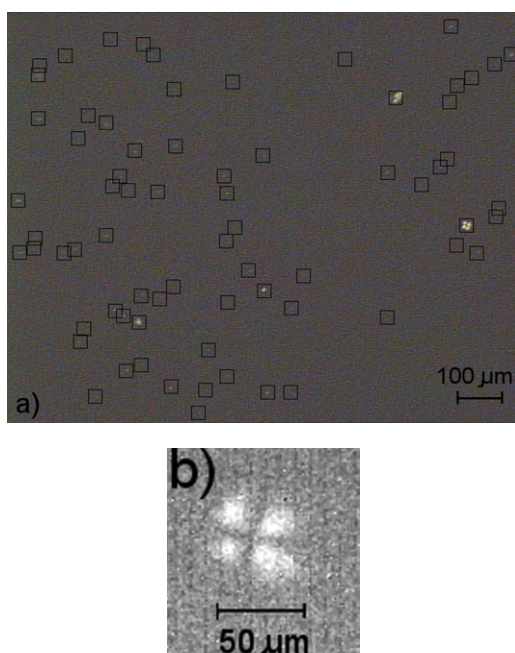


**Figure 5.** Polarized microscopy images of (a) CNT loaded LC cell showing some light through the points where the director is deformed. Dark squares mark most noticeable points of deformation. (b) director deformation under crossed polarizers.

particle in a solvent,  $D$ , is related to the hydrodynamic diameter of the particles  $d_h$  by the Stokes–Einstein equation [28, 30]

$$d_h = \frac{kT}{3\pi\eta D},$$

where  $k$  is Boltzmann’s constant;  $T$  is the absolute temperature;  $\eta$  is the viscosity.

The hydrodynamic diameter refers to how a particle diffuses within a fluid [31]. The translational diffusion coefficient depends not only on the size of the particle ‘core’ but also on any surface structure, as well as the concentration and type of ions in the medium [31]. In general, light scattering particle-sizing techniques have an inherent problem in describing the size of non-spherical particles [32]. If the shape of a particle changes in a way that affects the

diffusion speed, then the hydrodynamic size will change. Here we assume that the hydrodynamic diameter of a rod-shaped particle is effectively a sphere created by the rotation of the particle, and if  $d_l$  is the length of a rod-shaped particle and  $d_r$  is its diameter,  $d_h \geq (d_l + 2d_r)/3$ .

The dynamic light scattering (DLS), also referred to as photon correlation spectroscopy or quasi-elastic light scattering, allows measurement of particle sizes in suspensions with a broad range of sizes (from sub-nanometre to several micrometres) [28, 33, 34]. DLS measures the diffusion coefficient by probing the rate of fluctuation of the scattered light [28]. This technique benefits from statistical data averaging. However, it has limited size resolution. If the size ratio of two particles is smaller than 3 : 1, they will show as one with an intermediate size [31]. There is the possibility of relating the scattering results to the concentration of particles, although to the best of our knowledge this has not been implemented in any commercially available instruments. The sensitivity of the system depends on particle size. The smaller the particle, the weaker the scattered signal it produces. The intensity of the scattered signal versus size is proportional to the 6th power of its diameter [35]. Therefore, very small particles can be registered only if present at high concentrations or without large particles to mask the signal.

Depolarized dynamic light scattering (DDLS) is similar to DLS, but only the light scattered from anisotropic particles and, therefore, of different polarization, is collected. [15]. This technique was previously used to monitor length and diameter of CNT bundles and to study the influence of ultrasonication time and power on resulting suspension quality in CNT dispersions with surfactants in water (0.3 wt% concentration) [15]. However, DDLS can be used when particle concentration is large enough to obtain sizeable signal scattered into another polarization.

Another technique, nanoparticle tracking analysis (NTA) is based on directly observing scattering from nanoparticles in suspension and analysing the Brownian motion of each particle [36]. A laser beam is passed through the suspension and scattered light perpendicular to the laser beam is observed through a microscope. The field of view is video recorded by a camera over a period of time (30 s–5 min). The video

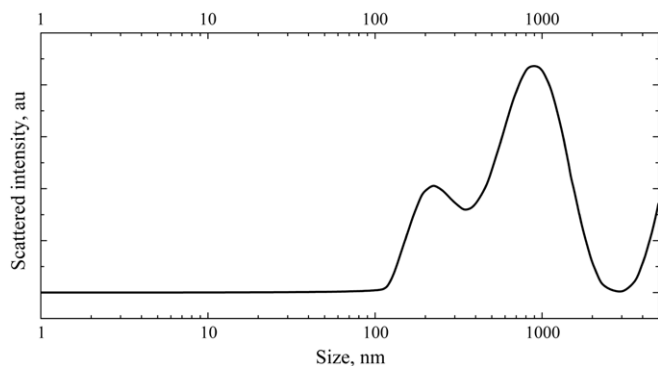


**Figure 6.** Size distribution of particles in the dispersion of octadecylamine functionalized CNTs in E7, dynamic light scattering method.

files are processed and each particle trajectory is tracked and analysed by software. The information collected about the number and diffusion behaviour of nanoparticles is used to derive their concentration and size distribution. The minimum detectable size depends on the particle refractive index and can be as low as 9–15 nm for high refractive index materials such as colloidal silver [37]. The maximum size that can be accurately measured is 1000 nm [29]. For a statistically significant number of particles to be present in the beam, sample concentrations should be above  $10^7$  particles  $\text{ml}^{-1}$  [38]. The system resolves closely sized particles and is better suited for poly-disperse samples than DLS. However, in the case of CNTs, the size along their axis may be approaching the upper limit of particle size that can be detected.

We use both nanoparticle tracking and DLS to study the equilibrated LC–CNT mixture already characterized by AFM, TEM and optical microscopy, as described above. To do so, a LC–CNT mixture is dissolved in acetone or hexane to suppress scattering due to the nematic phase.

A DLS system Zetasizer Nano ZS from Malvern is used for DLS studies. A measurement on solution of E7 LC in acetone (reference sample) detects particles with hydrodynamic diameter  $\sim 1.6$  nm. The E7 LC host is a 4 component mixture of 4-pentyl-4'-cyanobiphenyl, 4-heptyl-4'-cyanobiphenyl, 4-octyloxy-4'-cyanobiphenyl and 4-pentyl-4'-cyanoterphenyl [12, 39]. We estimate the average size of these molecules to be  $d_r \sim 0.3$  nm,  $d_l \sim 2$  nm. It is highly likely that the particles with the hydrodynamic diameter of 1.6 nm registered in the above measurement are E7 molecules.

The measurement of the hydrodynamic diameter of the sample loaded with CNTs has two major peaks: around 200 and 900 nm (figure 6). Another rise in intensity above  $3 \mu\text{m}$  may be due to larger CNT clumps or some other contamination. These peaks mask the weaker signal from small LC molecules. Note that the larger the particle, the stronger the scattering signal it produces. From figure 6, the intensity ratio between 200 nm and 900 nm peaks is 1 : 2. This translates to a number density of more than 2000 : 1 i.e. for each 900 nm particle there are 2000 particles with 200 nm hydrodynamic diameter. Therefore, in this particular system there are more particles with hydrodynamic diameter  $\sim 200$  nm.

NTA is performed using the NanoSight LM10 particle tracking system. Pure LC reference solutions in hexane give no

scattering. ODA functionalized CNT equilibrium suspensions in LC dissolved in hexane show  $\sim 4 \times 10^7$  particles  $\text{ml}^{-1}$  (volume fraction  $\sim 3 \times 10^{-11}$  and weight fraction  $\sim 10^{-10}$  wt) with mean effective hydrodynamic particle size  $\sim 200$  nm and size distribution 80–380 nm. All test suspensions are filtered through a  $0.45 \mu\text{m}$  filter prior to the investigation.

Both measurements are in a good agreement with the AFM studies described above ( $10^8$  particles  $\text{ml}^{-1}$ ,  $10^{-9}$  wt, bundle sizes  $\sim 6 \text{ nm} \times 500 \text{ nm}$ ). CNTs have highly anisotropic shape, and their effective diameter is expected to be smaller than their actual length. The larger sized particles detected by DLS may correspond to clumps of nanotubes. They are not detected using NTA, because in this case the mixtures are filtered using  $0.45 \mu\text{m}$  pores. We do not register any signal from the individual  $\sim 1$ – $3$  nm catalyst nanoparticles. This is below the resolution limit for our equipment. In DLS the signal from larger nanotubes and bundles would have masked the predictably weak signal from a relatively dilute concentration of  $\sim 1$ – $3$  nm nanoparticles (as from Mie theory the intensity of the scattered signal scales as  $r^6$  [35]).

DLS and its depolarized version are perhaps the fastest and most sensitive techniques for assessing the quality of dispersions. They require small samples, but the sample has to be either heated to the isotropic state, or diluted in another solvent to destroy the LC scattering phase. Adding solvents makes systems more difficult to analyse, as a strong change in viscosity of the mixture may lead to CNT aggregation and poor results from initially good dispersions. Therefore a lot of care should be taken when choosing a solvent.

### 3.4. Resonant Raman spectroscopy

Raman spectroscopy is a fast and non-destructive method for the characterization of carbon materials, nanotubes in particular [40]. Recently, resonant Raman spectroscopy was used to characterize CNTs in liquid crystalline matrices [41, 42]. These were 0.01 wt% dispersions of HiPco single-wall CNTs in E7 LC in planar aligned  $10 \mu\text{m}$  films.

In the  $1550$ – $1590 \text{ cm}^{-1}$  region, the Raman spectra of SWNTs are characterized by the presence of two distinct features: the so-called  $G^+$  and  $G^-$  peaks. These originate from the tangential (TO) and the longitudinal (LO) modes derived from the splitting of the  $E_{2g}$  phonon of graphene [43]. In metallic tubes, the LO mode is affected by a Kohn anomaly (KA), which causes the softening of this phonon [43, 44]. Since KA are not present in semiconducting SWNTs, the  $G^+$ ,  $G^-$  assignment in metallic SWNTs is the opposite of semiconducting tubes (the  $G^-$  peak is the LO mode in metallic and TO in semiconducting) [43, 44]. In semiconducting tubes, both the  $G^+$  and the  $G^-$  peaks appear as sharp Lorentzians. The  $G^+$  peak is usually more intense than the  $G^-$ , and its position is nearly independent of the tube's diameter, whereas the position of the  $G^-$  peak decreases for decreasing tube diameter [43, 44]. On the other hand, in metallic tubes, the  $G^-$  peak is usually rather intense, very broad, and downshifted with respect to its counterpart in semiconducting tubes [43]. Doping changes peaks' positions and widths [45, 46].

The other prominent features in Raman spectrum of CNTs are the radial breathing modes (RBMs) [47]. The

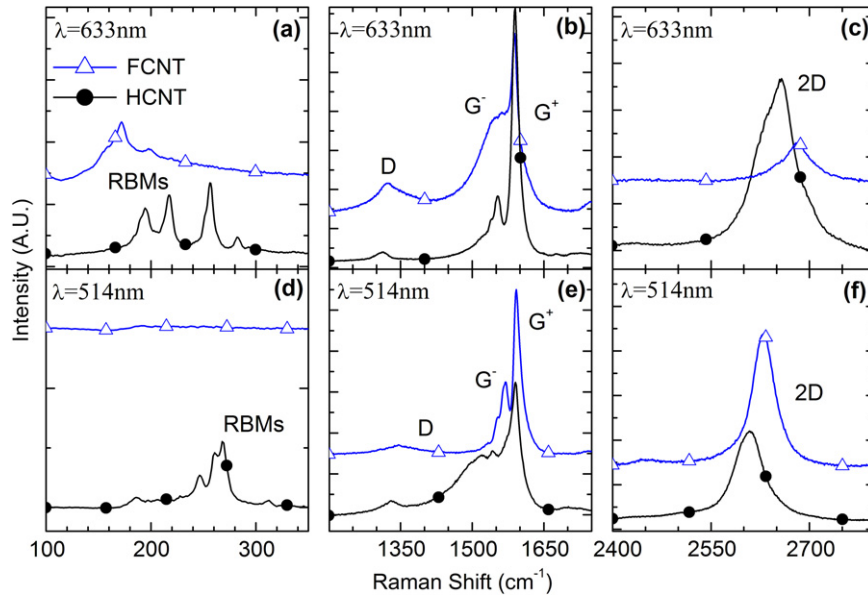


**Figure 7.** Raman spectra of HCNT and FCNT powders at 514 and 633 nm excitations. (a), (d) RBM (b), (e) G band (c), (f) 2D peak region.

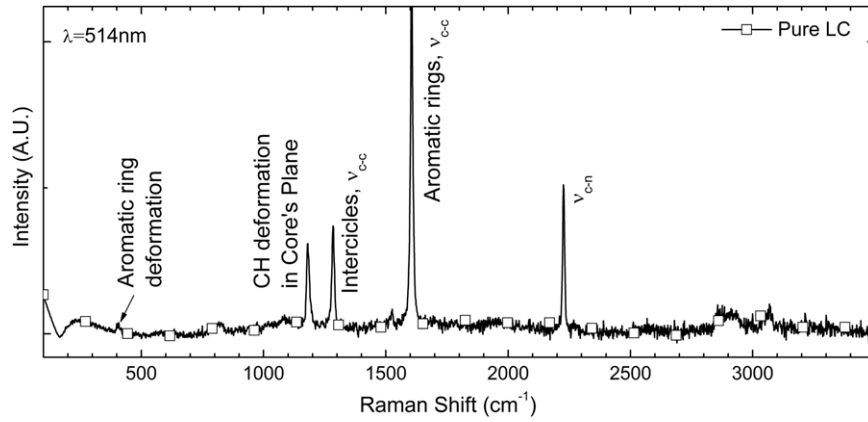


**Figure 8.** Raman spectrum of LC material at 514 nm excitation.

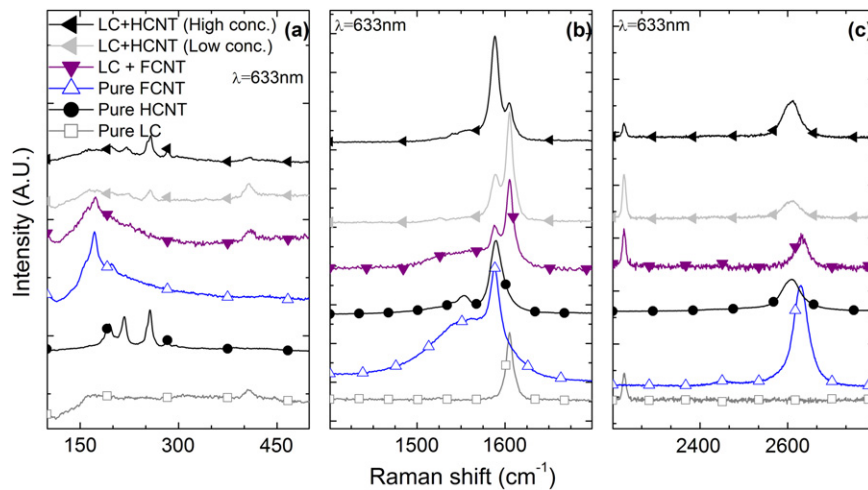


**Figure 9.** Raman spectra from unequilibrated aligned LC films loaded with HCNTs and FCNTs. (a) RBMs, (b) G band, (c) 2D peak. Raman spectra from pure FCNTs, HCNTs and LC material are included for comparison.

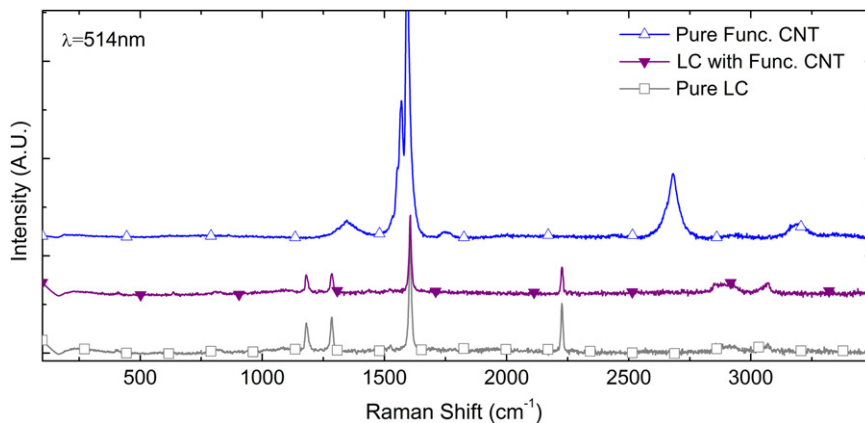


**Figure 10.** Raman spectrum from LC loaded with FCNTs (equilibrated). Spectra from pure LC and pure FCNT powders are also included for comparison.

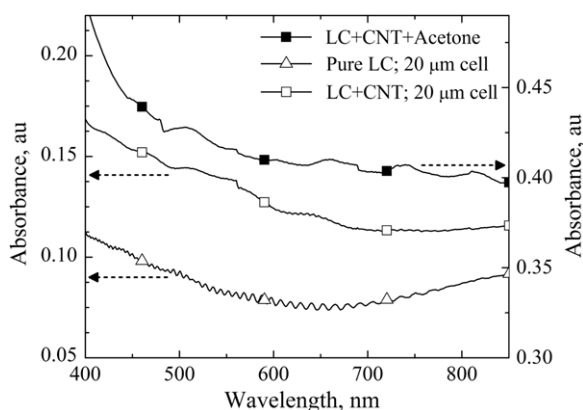


**Figure 11.** Absorption spectra of LC samples loaded with CNTs.

SWNT diameter can be derived from the RBM frequency:  $d = C_1/(\omega_{\text{RBM}} - C_2)$ , combined with the Kataura plot [48–50] and the excitation energy. A variety of different  $C_1$  and  $C_2$  values have been proposed [48–51] but their precise values are only critical for chirality assignment. Here we use  $C_1 = 214.4 \text{ cm}^{-1}$  and  $C_2 = 18.7 \text{ cm}^{-1}$  [51].

Raman spectra are measured with a Renishaw 1000 spectrometer at 514 (2.41 eV) and 633 (1.96 eV) nm using a  $50\times$  objective with an incident power of  $\sim 2 \text{ mW}$  and 30 s acquisition time. We stress that due to the cutoff of our notch filter, we cannot detect CNT diameters above 2 nm. In addition to equilibrated ODA functionalized CNT dispersions in E7 we also study unequilibrated dispersions of unfunctionalized HiPco CNTs in E7, as in [41, 42]. In this section, we refer to functionalized CNTs as FCNTs and HiPco single-wall CNTs as HCNTs.

Figure 7 shows Raman spectra of HCNT and FCNT powders at 514 and 633 nm excitations. For HCNTs, a lorentzian fit gives  $G^+$  and  $G^-$  peaks at  $\sim 1590 \text{ cm}^{-1}$ ,  $1552 \text{ cm}^{-1}$  and at  $\sim 1591 \text{ cm}^{-1}$ ,  $1520 \text{ cm}^{-1}$  for 633 nm and 514 nm excitations, respectively. In the case of FCNTs, these values are  $\sim 1588 \text{ cm}^{-1}$ ,  $1552 \text{ cm}^{-1}$  and  $\sim 1592 \text{ cm}^{-1}$ ,  $1567 \text{ cm}^{-1}$ . Combining the Kataura plot [48–50] with the excitation energy, it can be deduced that the RBMs in figure 7(a) (at  $\sim 194$ , 217, 256 and  $282 \text{ cm}^{-1}$ ) from 633 nm

excitation in HCNT samples are from both semiconducting and metallic CNTs, with a diameter range from 0.8 to 1.2 nm. On the other hand, the 514 nm excitation on HCNT samples mostly probes metallic nanotubes with RBMs at 247, 261 and  $268 \text{ cm}^{-1}$  ( $\sim 0.8$ – $1.0 \text{ nm}$  diameter); see figure 7(e). We only observe a weak RBM signal at  $187 \text{ cm}^{-1}$  from semiconducting tubes. The shape of  $G^-$  peaks of HCNTs also indicates that mostly semiconducting SWNTs are measured at this excitation [43].

In the case of the FCNTs, we observe RBMs only for 633 nm excitation. The predominant RBM peaks at  $\sim 175$  and  $199 \text{ cm}^{-1}$  are from metallic nanotubes with  $\sim 1.3 \text{ nm}$  diameter. This is also reflected in the shape of  $G^-$  peak [43]. We do not observe any RBMs from FCNTs at 514 nm excitation. We observe a large up-shift ( $\sim 25 \text{ cm}^{-1}$ ) in the 2D peak in the FCNTs compared with HCNTs, see figures 7(c) and (f). This could be due to hole-doping of ODA functionalized SWNTs, FCNTs [52, 53].

The Raman spectrum of pure LC at 514 nm excitation is presented in figure 8. The observed Raman peaks [54–56] are from the constituent cyanobiphenyls (CB) and cyanoterphenyls (CT) of the E7 LC material [25, 56, 57] and are assigned according to [54–56]. The orientation order of LCs can be usually monitored using the  $C \equiv N$  stretching band at  $2226 \text{ cm}^{-1}$  [56, 58]. This band is important in determining LC orientation since it is highly polarized and the direction of this vibration is parallel to the mean LC director [58]. The  $1603 \text{ cm}^{-1}$  band due to C–C stretching of aromatic rings has also been used to characterize orientation of LCs and of CNTs dispersed in LCs [18, 41, 59].

Raman spectroscopy is used to characterize samples of  $14 \mu\text{m}$  planar aligned films of LC loaded with  $\sim 0.01 \text{ wt\%}$  FCNTs and HCNTs (non-equilibrated). As in [41], presence of CNTs (both FCNTs and HCNTs) is detected, see figure 9. Due to higher concentration than the equilibrated mixtures, the CNTs in these films form microscopic aggregates on which the Raman measurements can be taken. In these samples, uniform areas without any apparent CNT aggregation under optical microscope do not yield any Raman peaks from CNTs under the same measurement conditions. This is similar to our observation from equilibrated aligned LC films loaded

**Table 1.** The results from the different techniques characterising E7 LC loaded with ODA functionalized CNTs.

Method	Concentration	Size	Comment
AFM	$4 \times 10^8$ particles ml <sup>-1</sup> ( $7.4 \times 10^{-9}$ wt)	300–1900 nm average $\sim 500$ nm	On filter $0.2 \mu\text{m}$ pore size
Optical microscopy	$\sim 10^9$ particles ml <sup>-1</sup> ( $4 \times 10^{-9}$ wt)	n/a	In aligned $20 \mu\text{m}$ cell sizing not possible
NTA	$\sim 4 \times 10^7$ particles ml <sup>-1</sup> ( $\sim 10^{-10}$ wt)	$\sim 200$ nm	In solvent, $0.45 \mu\text{m}$ filter
DLS	n/a but potentially possible	$\sim 200$ nm and $\sim 900$ nm	In solvent

**Table 2.** Techniques for monitoring LC–CNT dispersions.

Method	Sample required	Range	Applicability and limitations
Resonant Raman spectroscopy	Planar LC cell	<i>CNT and LC</i> 0.001 wt% CNT in LC [41, 42]	Sensitive to exciting beam polarization
Optical microscopy	LC cell	<i>LC specific</i> Min $10^5$ particles ml <sup>-1</sup> ( $3 \times 10^{-13}$ wt), $\times 50$ magnification $100 \mu\text{m}$ cell	Contamination must be minimized
AFM	On filter	<i>Scanning probe microscopy</i> $\sim 10^5$ particles ml <sup>-1</sup> or lower concentrations	Particle size must be larger than filter pore size; limited area of scan <sup>a</sup> ;
ESEM	On filter	$\sim 10^5$ particles ml <sup>-1</sup>	Limited area of scan <sup>a</sup> ; substrates limit the use of high power beam
TEM	Bulk deposited on grid	<i>Electron microscopy</i> $\sim 10^5$ particles ml <sup>-1</sup>	Limited area of scan <sup>a</sup> , suitable for particles down to 1 nm
Absorption (Vis, IR)	Isotropic phase (solvent or heating)	<i>Spectroscopy (for absorbing dopants)</i> 0.001 wt% (in D <sub>2</sub> O) [14, 61]	LCs need heating to $>70$ – $110^\circ\text{C}$ or careful solvent selection
Nanoparticle Tracking Analysis [29, 36]		<i>Elastic scattering</i> Min $10^7$ particles ml <sup>-1</sup> ( $3 \times 10^{-11}$ wt); size 10–1000 nm;	Detects concentration, dopant size distribution; limited by number of scattering centres in view LCs needs heating to $70$ – $110^\circ\text{C}$ or careful solvent selection
Dynamic light scattering [31]	Isotropic phase (solvent or heating)	$0.6 \text{ nm}$ – $6 \mu\text{m}$ ;	Detects dopant size distribution; limited by detector sensitivity/contamination LCs need heating to $>70$ – $110^\circ\text{C}$ or careful solvent selection
Depolarized dynamic light scattering		Reported studies of $0.3 \text{ wt}\%$ aqueous CNT dispersion [15]	Detects anisotropic dopant size and shape; limited by detector sensitivity LCs need heating to $>70$ – $110^\circ\text{C}$ or careful solvent selection

<sup>a</sup> Area of scan should be no larger than  $10 \times 10 \mu\text{m}^2$  to resolve CNT bundles and less than  $1 \times 1 \mu\text{m}^2$  to resolve individual nanotubes.

with CNTs; to be discussed later. RBMs between  $200$  and  $300 \text{ cm}^{-1}$  and at  $\sim 175 \text{ cm}^{-1}$  are detected in the HCNT and FCNT loaded LCs, respectively, similar to the pure HCNT and FCNT powders; see figure 9(a). As seen from figure 9(b), the CNT G<sup>+</sup> peak is very close to the C–C stretching of aromatic rings of the LC material ( $\sim 1603 \text{ cm}^{-1}$ ) [54]. Samples loaded with FCNTs and HCNTs exhibit the distinct G<sup>+</sup> peak from CNTs at  $\sim 1590 \text{ cm}^{-1}$ , and a weak G<sup>-</sup> peak. In figure 9(c), the C  $\equiv$  N stretching band can be observed in all the samples containing the LC material. Additionally, the 2D

peak from CNTs is seen from samples containing both FCNTs and HCNTs.

We also employ Raman spectroscopy to characterize samples of  $20 \mu\text{m}$  planar aligned pure LC films and films of equilibrated dispersions of FCNTs in LC. Unlike the samples discussed above, no FCNT aggregation is visible under the optical microscope. Figure 10 shows the Raman spectra of the aligned LC films loaded with equilibrated FCNTs at  $514 \text{ nm}$  excitation. For ease of comparison, Raman spectra of pure LC and of FCNT powder are reproduced in the same figure. The

spectra of pure LC and equilibrated LC loaded with FCNTs perfectly overlap. Moreover, no distinct Raman peak from the FCNTs in the FCNT–LC sample is observed. This suggests that the equilibrated dispersions of FCNTs in LC have too low concentration to be detected by Raman spectroscopy in our measurement conditions.

### 3.5. Absorption spectroscopy

Absorption spectroscopy is a versatile tool for characterization of optical materials. CNTs have highly anisotropic absorption (dichroism), and their alignment can be studied by polarized light [60]. Absorption can be used to characterize CNT dispersions in films or in dispersions in D<sub>2</sub>O (deuterium oxide, in contrast to water, does not absorb in the infrared) [14, 61]. Nematic LC phases in bulk form have non-uniform refractive index and cause strong light scattering [62]. Aligned LC cells do not provide sufficient beam path length for an appreciable absorption in dispersions with low CNT loading. To increase beam path length, cuvettes must be used. Also, solvents (e.g. acetone) might be used to transform studied material into transparent isotropic phases.

Absorption spectroscopy of cells produces results with interference because the small gap between the glass plates acts as an interferometric structure. We observe very weak but distinct absorption peaks from cells prepared with CNTs dispersed in LCs (figure 11). These absorption peaks are from  $E_{22}$  of semiconducting and  $E_{11}$  of metallic nanotubes [10]. To confirm they are indeed from CNTs, we dilute CNT–LC mixtures with acetone (1:6) to transform the mixture into isotropic phases. Indeed, we observe similar peaks in the diluted mixture, with stronger intensity. The shifts in the absorbance peak positions are probably due to the different dielectric environment surrounding the CNTs [63, 64]. It is therefore possible to detect CNTs in dispersions and in cells. However, in these samples, the CNT concentration is very close to the minimum detection limit of the equipment.

Table 1 shows the results of characterization of the studied E7+CNT system. Table 2 summarizes the discussed characterization techniques.

## 4. Conclusions

We explored various characterization avenues for CNT–LC dispersions. We have achieved  $\sim 10^{-9}$  wt% loading in equilibrated dispersions which is  $10^6$  times smaller than that quoted for water dispersions. This leaves scope for future improvement of the loading.

Four methods were found to be suitable for characterising such equilibrated and very dilute concentrations of CNTs in LC. These methods are AFM, optical microscopy, NTA and DLS. Optical microscopy is also convenient and informative; however, it does not provide direct information about the size of the particles and is sensitive to any contamination. Raman scattering is useful for higher loadings.

## Acknowledgments

OT and NC acknowledge financial support from the Centre for Advanced Photonics and Electronics (CAPE) and ALPS Electric. JG acknowledges funding from the European EXCELL project. ACF from the Royal Society, Brian Mercer Award for Innovation, Leverhulme and Newton Trusts and EPSRC grants GR/S97613/01, EP/E500935/1. The authors thank Patrick Hole of NanoSight Ltd for assistance with the NTA, Alex Winkel from Veeco Instruments Ltd for assistance with the AFM images, David Jefferson and Angel Berenguer for TEM, Trevor Fairhead and Jon J Rickard for ESEM studies.

## References

- [1] Collings P J and Hird M 1997 *Introduction to Liquid Crystals Chemistry and Physics* (London: Taylor and Francis)
- [2] Dierking I, Scalia G, Morales P and LeClere D 2004 Aligning and reorienting carbon nanotubes with nematic liquid crystals *Adv. Mater.* **16** 865–9
- [3] Lynch M D and Patrick D L 2002 Organizing carbon nanotubes with liquid crystals *Nano Lett.* **2** 1197–201
- [4] Khoo I C, Ding J, Zhang Y, Chen K and Diaz A 2003 Supra-nonlinear photorefractive response of single-walled carbon nanotube- and C60-doped nematic liquid crystal *Appl. Phys. Lett.* **82** 3587–9
- [5] Lee W and Chiu C-S 2001 Observation of self-diffraction by gratings in nematic liquid crystals doped with carbon nanotubes *Opt. Lett.* **26** 521–3
- [6] Trushkevych O, Collings N, Crossland P W A, Wilkinson T D, Georgiou A and Milne W I 2007 Projection of holograms from photorefractive OASLMs *J. Nonlinear Opt. Phys. Mater.* **16** 307
- [7] Huang C-Y, Hu C-Y, Pan H-C and Lo K-Y 2005 Electrooptical responses of carbon nanotube-doped liquid crystal devices *Japan. J. Appl. Phys.* **44** 8077–81
- [8] Lee W, Wang C-Y and Shih Y-C 2004 Effects of carbon nanosolids on the electro-optical properties of a twisted nematic liquid-crystal host *Appl. Phys. Lett.* **85** 513–5
- [9] Chen H-Y and Lee W 2006 Suppression of field screening in nematic liquid crystals by carbon nanotubes *Appl. Phys. Lett.* **88** 222105–3
- [10] O’Connell M J *et al* 2002 Band gap fluorescence from individual single-walled carbon nanotubes *Science* **297** 593
- [11] O’Connell M J *et al* 2001 Reversible water-solubilization of single-walled carbon nanotubes by polymer wrapping *Chem. Phys. Lett.* **342** 265–71
- [12] Moore V C *et al* 2003 Individually suspended single-walled carbon nanotubes in various surfactants *Nano Lett.* **3** 1379–82
- [13] Islam M F, Rojas E, Bergey D M, Johnson A T and Yodh A G 2003 High weight fraction surfactant solubilization of single-wall carbon nanotubes in water *Nano Lett.* **3** 269–73
- [14] Rozhin A G *et al* 2006 Generation of ultra-fast laser pulses using nanotube mode-lockers *Phys. Status Solidi b* **243** 3551–5
- [15] Badaire S, Poulin P, Maugey M and Zakri C 2004 In situ measurements of nanotube dimensions in suspensions by depolarised dynamic light scattering *Langmuir* **20** 10367–70
- [16] Sabba Y and Thomas E L 2004 High-concentration dispersion of single-wall carbon nanotubes *Macromolecules* **37** 4815–20
- [17] Huang Y Y, Ahir S V and Terentjev E M 2006 Dispersion rheology of carbon nanotubes in a polymer matrix *Phys. Rev. B* **73** 125422

- [18] Lagerwall J F P, Scalia G, Haluska M, Dettlaff-Weglikowska U, Giesselmann F and Roth S 2006 Simultaneous alignment and dispersion of carbon nanotubes with lyotropic liquid crystals *Phys. Status Solidi b* **243** 3046–9
- [19] Hasan T, Scardaci V, Tan P H, Rozhin A G, Milne W I and Ferrari A C 2007 Stabilization and ‘debundling’ of single-wall carbon nanotube dispersions in *N*-methyl-2-pyrrolidone (NMP) by polyvinylpyrrolidone (PVP) *J. Phys. Chem. C* **111** 12594–602
- [20] Tagmatarchis N and Prato M 2004 Functionalization of carbon nanotubes via 1,3-dipolar cycloadditions *J. Mater. Chem.* **14** 437–9
- [21] Torre Gdl, Blau W and Torres T 2003 A survey of the functionalization of single-walled nanotubes. The chemical attachment of phtalocyanine moieties *Nanotechnology*. **14** 765–71
- [22] Dodge R, Kang S-W, Kumar S, Park C and Siochi M (ed) 2006 Carbon nanotube liquid crystal composites *The American Physical Society Meeting (Baltimore, MD, USA, March 2006)*
- [23] [www.merck.de](http://www.merck.de)
- [24] <http://www.sigma-aldrich.com>
- [25] Rugar D and Hansma P 1990 Atomic force microscopy *Phys. Today* **43** 23–30
- [26] Wilkinson T D, Wang X, Teo K B K and Milne W I 2008 Sparse multiwall carbon nanotube electrode arrays for liquid-crystal photonic devices *Adv. Mater.* **20** 363–6
- [27] Jang C-H, Cheng L-L, Olsen C W and Abbott N L 2006 Anchoring of nematic liquid crystals on viruses with different envelope structures *Nano Lett.* **6** 1053–8
- [28] Pecora R 2000 Dynamic light scattering measurement of nanometer particles in liquids *J. Nanopart. Res.* **2** 123–31
- [29] Carr R, Diaper T and Barrett E 2005 NanoParticle Tracking Analysis—The Halo™ System. Particulate Systems Analysis (UK: Royal Society of Chemistry)
- [30] Berne B J and Pecora R 1976 *Dynamic Light Scattering* (New York: Wiley)
- [31] Nobbmann U and Kaszuba M 2007 Nanoparticle size characterisation *Malvern Instruments Seminar (Cambridge, UK, 18 April)*
- [32] Maragò O M *et al* 2008 Optical trapping of carbon nanotubes *Physica E* **40** 2347
- [33] Kaszuba M, McKnight D, Connah M T, McNeil-Watson F K and Nobbmann U 2008 Measuring sub nanometre sizes using dynamic light scattering *J. Nanopart. Res.* **10** 823–9
- [34] Kaszuba M 1999 The measurement of nanoparticles using photon correlation spectroscopy and avalanche photo diodes *J. Nanopart. Res.* **1** 405–9
- [35] Mie G 1908 Beiträge zur optik trüber medien, speziell kolloidaler metallösungen *Ann. Phys.* **4** 377–445
- [36] [www.nanosight.co.uk](http://www.nanosight.co.uk)
- [37] Barcikowski S, Menendez-Manjon A, Chichkov B, Brikas M and Raciukaitis G 2007 Generation of nanoparticle colloids by picosecond and femtosecond laser ablations in liquid flow *Appl. Phys. Lett.* **91** 083113
- [38] 2007 NanoSight. LM10 Nanoparticle Analysis System manual
- [39] Pestov S M, Serafimov L A and V. KE 2007 Thermodynamic modeling of liquid crystal—nonmesogen systems in the approximation of the theory of regular solutions *Theor. Found. Chem. Eng.* **41** 91–5
- [40] Ferrari A C and Robertson J (ed) 2004 Raman spectroscopy in carbons: from nanotubes to diamond *Phil. Trans. R. Soc. Lond. Ser. A*. **362** 2267
- [41] Lagerwall J F P, Scalia G, Haluska M, Dettlaff-Weglikowska U, Roth S and Giesselmann F 2007 Nanotube alignment using lyotropic liquid crystals *Adv. Mater.* **19** 359–64
- [42] Scalia G, Haluska M, Dettlaff-Weglikowska U, Giesselmann F and Roth S 2005 Polarized Raman spectroscopy study of SWNT orientational order in an aligning liquid crystalline matrix *Electronic Properties of Novel Nanostructures, 19th Int. Winterschool/Euroconf. on Electronic Properties of Novel Materials 2005 (Kirchberg, Austria)* (New York: American Institute of Physics) p 114–7
- [43] Piscanec S, Lazzeri M, Robertson J, Ferrari A C and Mauri F 2007 Optical phonons in carbon nanotubes: Kohn anomalies, Peierls distortions, and dynamic effects *Phys. Rev. B* **75** 035427
- [44] Piscanec S, Lazzeri M, Francesco M, Ferrari A C and Robertson J 2004 Kohn anomalies and electron–phonon interactions in graphite *Phys. Rev. Lett.* **93** 185503
- [45] Pisana S *et al* 2007 Breakdown of the adiabatic Born–Oppenheimer approximation in graphene. *Nat. Mater.* **6** 198–201
- [46] Caudal N, Saitta A M, Lazzeri M and Mauri F 2007 Kohn anomalies and nonadiabaticity in doped carbon nanotubes *Phys. Rev. B* **75** 115423–11
- [47] Jorio A *et al* 2005 Resonance Raman spectroscopy (*n, m*)-dependent effects in small-diameter single-wall carbon nanotubes. *Phys. Rev. B* **71** 075401
- [48] Telg H, Maultzsch J, Reich S, Hennrich F and Thomsen C 2004 Chirality distribution and transition energies of carbon nanotubes *Phys. Rev. Lett.* **93** 177401
- [49] Kataura H *et al* 1999 Optical properties of single-wall carbon nanotubes *Synth. Met.* **103** 2555–8
- [50] Fantini C, Jorio A, Souza M, Strano M S, Dresselhaus M S and Pimenta M A 2004 Optical transition energies for carbon nanotubes from resonant raman spectroscopy: environment and temperature effects *Phys. Rev. Lett.* **93** 147406
- [51] Telg H, Maultzsch J, Reich S and Thomsen C 2006 Resonant-Raman intensities and transition energies of the  $E_{11}$  transition in carbon nanotubes. *Phys. Rev. B* **74** 115415–5
- [52] Yang Y Y, Chen S W, Xue Q B, Biris A and Zhao W 2005 Electron transfer chemistry of octadecylamine-functionalized single-walled carbon nanotubes *Electrochim. Acta* **50** 3061–7
- [53] Das A *et al* 2007 Probing the doping in metallic and semiconducting carbon nanotubes by Raman and transport measurements (*Preprint 0709.27v1*) (cond-mat mes-hall)
- [54] Kang D S *et al* 2005 Temperature-dependent Raman spectroscopic study of the nematic liquid crystal 4-*n*-pentyl-4'-cyanobiphenyl *Appl. Spectrosc.* **59** 1136–40
- [55] Fehr C, Dieudonne P, Sauvajol J L and Anglaret E 2003 Raman investigation of stable and metastable states of 4-octyl-4'-cyanobiphenyl confined in porous silica matrices *Phys. Rev. E* **67** 061706
- [56] Gray G W and Mosley A 1976 Raman-spectra of 4-cyano-4'-pentylbiphenyl and 4-cyano-4'-pentyl-D11-biphenyl *Mol. Cryst. Liq. Cryst.* **35** 71–81
- [57] Seo D S, Nishikawa M and Kobayashi S 1997 Generation of high pretilt angles of nematic liquid crystal (5CB) on rubbed organic solvent soluble polyimide surfaces with helical backbone structure and trifluoromethyl moieties *Liq. Cryst.* **22** 515–7
- [58] Blach J F, Daoudi A, Buisine J M and Bormann D 2005 Raman mapping of polymer dispersed liquid crystal *Vib. Spectrosc.* **39** 31–6
- [59] Scalia G, Lagerwall J P F, Schymura S, Haluska M, Giesselmann F and Roth S 2007 Carbon nanotubes in liquid crystals as versatile functional materials *Phys. Status Solidi b* **244** 4212–7
- [60] Ichida M, Mizuno S, Kataura H, Achiba Y and Nakamura A 2004 Anisotropic optical properties of mechanically aligned

- single-walled carbon nanotubes in polymer *Appl. Phys. A* **78** 1117–20
- [61] Lebedkin S, Arnold K, Hennrich F, Krupke R, Renker B and Kappes M M 2003 FTIR-luminescence mapping of dispersed single-walled carbon nanotubes *New J. Phys.* **5** 140
- [62] De Jeu W H 1980 *Physical Properties of Liquid Crystalline Materials* (London: Gordon and Breach)
- [63] Perebeinos V, Tersoff J and Avouris P 2004 Scaling of excitons in carbon nanotubes *Phys. Rev. Lett.* **92** 257402
- [64] Walsh A G *et al* 2007 Screening of excitons in single, suspended carbon nanotubes *Nano Lett.* **7** 1485–8